HHS Public Access

Author manuscript

Biomacromolecules. Author manuscript; available in PMC 2016 February 12.

Published in final edited form as:

Biomacromolecules. 2016 February 8; 17(2): 415–426. doi:10.1021/acs.biomac.5b01210.

Toughening of Thermoresponsive Arrested Networks of Elastin-Like Polypeptides To Engineer Cytocompatible Tissue Scaffolds

Matthew J. Glassman[†], **Reginald K. Avery**[§,‡,∥,⊥], **Ali Khademhosseini**[§,∥,⊥], and **Bradley D. Olsen**[†,*]

[†]Department of Chemical Engineering, Massachusetts Institute of Technology, Cambridge, Massachusetts 02139, United States

[‡]Department of Biological Engineering, Massachusetts Institute of Technology, Cambridge, Massachusetts 02139, United States

[§]Biomaterials Innovation Research Center, Department of Medicine, Brigham and Women's Hospital, Harvard Medical School, Cambridge, Massachusetts 02139, United States

[∥]Wyss Institute for Biologically Inspired Engineering, Harvard University, Boston, Massachusetts 02115, United States

[⊥]Harvard–MIT Division of Health Sciences and Technology, Massachusetts Institute of Technology, Cambridge, Massachusetts 02139, United States

Abstract

Formulation of tissue engineering or regenerative scaffolds from simple bioactive polymers with tunable structure and mechanics is crucial for the regeneration of complex tissues, and hydrogels from recombinant proteins, such as elastin-like polypeptides (ELPs), are promising platforms to support these applications. The arrested phase separation of ELPs has been shown to yield remarkably stiff, biocontinuous, nanostructured networks, but these gels are limited in applications by their relatively brittle nature. Here, a gel-forming ELP is chain-extended by telechelic oxidative coupling, forming extensible, tough hydrogels. Small angle scattering indicates that the chain-extended polypeptides form a fractal network of nanoscale aggregates over a broad concentration range, accessing moduli ranging from 5 kPa to over 1 MPa over a concentration range of 5–30 wt %. These networks exhibited excellent erosion resistance and allowed for the diffusion and release of encapsulated particles consistent with a bicontinuous, porous structure with a broad distribution of pore sizes. Biofunctionalized, toughened networks were found to maintain the viability of human mesenchymal stem cells (hMSCs) in 2D, demonstrating signs of osteogenesis even in cell media without osteogenic molecules. Furthermore, chondrocytes could be readily mixed into these gels via thermoresponsive assembly and remained viable in extended culture. These studies

[*]**Corresponding Author**: bdolsen@mit.edu.

Supporting Information

The Supporting Information is available free of charge on the ACS Publications website at DOI: 10.1021/acs.biomac.5b01210. Additional details including complete sequences of proteins used in the study; supplemental tensile testing data and schematics; SAXS modeling details; large amplitude oscillatory shear rheology; staining images of MSCs in osteoinductive media and chondrocytes in 2D and in gels; and additional methods and materials for in vitro studies (PDF)

Notes

The authors declare no competing financial interest.

demonstrate the ability to engineer ELP-based arrested physical networks on the molecular level to form reinforced, cytocompatible hydrogel matrices, supporting the promise of these new materials as candidates for the engineering and regeneration of stiff tissues.

Graphical abstract

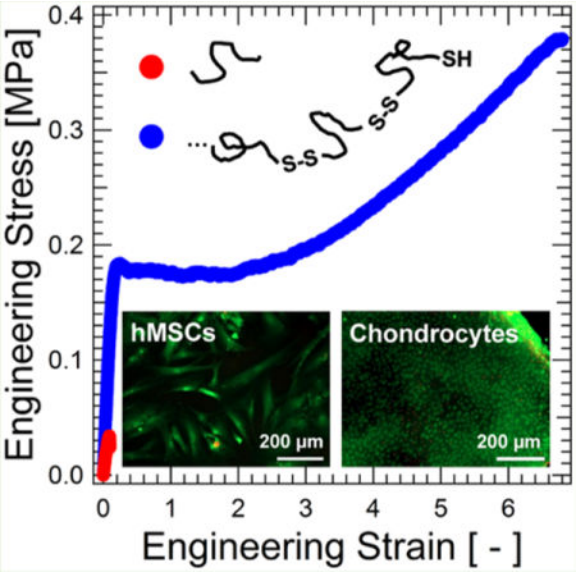

INTRODUCTION

Synthetically simple biomaterials that can be formulated under mild conditions are highly desired for biomedical applications.[1] For complex surgical interventions thought to be crucial for tissue regeneration, the chemistry, structure, and mechanical behavior of substrates must be suitable for clinical implantation and long-term performance under physiological conditions.[2–5] For example, in the injectable delivery of viscoelastic solids containing encapsulated cellular and molecular cargo, a candidate biomaterial must be able to flow through a narrow needle or cannula and then quickly form a solid in the tissue with the desired stiffness, porosity, and biodegradability for the target treatment regimen.[4,6–8] This strategy has been evaluated as a method to regenerate articular cartilage,[9] to guide spinal cord repair,[10] or to heal critical-size craniofacial defects.[11,12] Acellular bulking agents are also important to reinforce urological tissues to treat incontinence, prolapse, or preterm birth.[13] Responsive physical hydrogels are promising for a number of injectable applications as they can be prepared as viscoelastic liquids or shear-thinning solids and will rapidly assemble or self-heal in vivo to form solid implants postinjection.[14] However, for use in load-bearing tissues, it would be advantageous for injectable substrates to rapidly reform into tough implants with similar mechanical behavior to the target site in order to reduce premature degradation. The procedure for homogeneously encapsulating delicate cargo in soft matrices is similarly demanding: cells or drugs must be mixed as a liquid-like formulation that can rapidly transition into a solid with suitable mechanical properties for performance in the desired application.[7]

Achieving the large change in rheological properties necessary for long-term use of injectable materials or cell-laden matrices in muscle, cartilage, or bone is an ongoing challenge in biomaterials development. Recently, it was discovered that thermoreversible physical hydrogels with shear moduli of ca. 1 MPa can be prepared from moderately concentrated solutions of certain elastin-like polypeptides (ELPs),[15] yielding synthetically simple formulations that could potentially be used as novel substrates for engineering or regenerating stiff tissues. ELPs, artificial biomimetic polypeptides consisting of many repeats of the canonical pentapeptide VPGVG, exhibit an inverse temperature transition in aqueous solutions to become insoluble in water when heated.[16–19] The ELP sequence can tolerate a variety of amino acid substitutions in the repeat while retaining their thermoresponsive behavior.[20,21] In general, hydrophobic collapse of the polypeptide chain leads to the formation of a coacervate phase that readily macrophase-separates from solution. However, when ELPs with the sequence $([I^{0.2}V^{0.8}]\text{-PAVG})_n$ are prepared at concentrations above ca. 15 wt % in water, the typical process of domain coalescence and macroscopic phase separation is arrested, forming a semiperiodic nanoscale network of a dense polypeptide phase.[15] The structure, mechanics, and mechanism of network formation have been characterized in detail. While this newly discovered mechanism of responsive gelation for ELPs is potentially useful for applications in encapsulation and injectable delivery, the network that forms is fairly brittle. The ability to toughen these networks is a crucial step needed to advance the utility of this novel class of ELP hydrogels.

The toughening of soft materials has been demonstrated with various strategies, including double-networks,[22] interpenetrating networks,[23,24] nanocomposites,[25,26] and chain-extension.[27] In double-network gels, a loosely cross-linked network interacts with a densely cross-linked network in which sacrificial bonds are used to dissipate energy and relieve network inhomogeneities, suppressing crack propagation.[28] For chemical double-networks, this mechanism cannot be cycled indefinitely due to irreversible chain scission, but when sacrificial bonds are formed by physical interactions, network self-healing can enable cyclic nonlinear loading.[29,30] Interpenetrating networks have structural similarities to double-network gels, but are mechanically reinforced by the effects of finite chain extensibility in the primary network due to swelling of a charged secondary network.[31] Nanocomposites are formed by physical blending of a nanoparticulate filler into a soft matrix, introducing many mechanisms of network toughening including crack deflection, crack bridging, and distributing macroscopic stress among many molecules in the soft matrix. Chain-extension, a strategy found in many natural biomaterials, including mucus[32] and flour,[33] involves the coupling of telechelic polymeric substituents, resulting in a significant increase in the average molecular weight of matrix components. This process introduces physical entanglements that can span large distances in the soft matrix. An important advantage of chain extension is that it can be easily implemented in protein-based materials via introduction of cysteine residues near the N- and C-termini of a candidate protein sequence, allowing the original polymer to be extended via oxidative coupling of the thiol functional groups.[27]

In this work, oxidative chain-extension of telechelic ELPs is employed to toughen the responsively assembled, phase-separated protein network, leading to stiff, extensible, and highly hydrated biomaterials. Solutions of chain-extended ELPs are viscoelastic liquids

below the transition temperature, but form clear gels when heated to physiological temperatures at sufficiently high concentrations, with moduli greater than 1 MPa at 30 wt %. These gels exhibit scattering consistent with a fractal network of nanoscale aggregates, forming a bicontinuous network with a broad range of pore sizes. Furthermore, the gels exhibit improved recovery in cyclic large amplitude oscillatory shear measurements, ultimately withstanding greater peak stress prior to failure. Crucially, the gelation mechanism is also found to tolerate genetically encoded modifications including bioactive peptides such as cell-adhesion ligands. The cytocompatibility of these tough, functionalized biomaterials is investigated, demonstrating the ability to maintain the viability of hMSCs. The gels are also weakly osteoinductive and can maintain the viability of bovine chondrocytes mixed into the gels.

EXPERIMENTAL METHODS

Genetic Engineering and Biosynthesis

To leverage the arrested phase separation of ELPs to engineer tough biomaterials, the tolerance of this gelation mechanism to telechelic modifications of the polypeptide and chain extension polymerization was explored by the addition of sequences encoding biofunctional (i.e., containing RGDS) and toughening moieties (i.e., containing cysteine residues for oxidative chain extension). These modifications were introduced onto the N- and C-termini of the ELP $([I^{0.6}V^{0.4}]PAVG)_{50}$ using a one-step ligation strategy (Table 1). Telechelic ELPs with flanking sequences containing cysteine and cell adhesive sites were produced in a 4-component ligation reaction based on genetic elements synthesized previously:[15] (1) an adapted pET-28b vector (pETA), with a modified MCS containing a *Bam*HI and NheI site on the 5′ end, and a SpeI and *Hin*dIII site on the 3′ end; (2) an ELP gene flanked by NheI and SpeI sites encoding 50 repeats of the XPAVG pentapeptide, where X consists of isoleucine or valine in a 3:2 ratio; (3) an annealed pair of oligonucleotides for the 5′ modifications; and (4) an annealed pair of oligonucleotides for the 3′ modifications. Annealed oligonucleotide pairs were designed to have the appropriate overhangs for programmed assembly of the N- and C-terminal modifications. The following unphosphorylated oligonucleotides were annealed to form the 5′ pair:

N_for:
GATCCAAATGTACCTCTGCCGGCGCTGGTGCGGGCCCGGAAGGTCGTGGTG
ATTCTA

N_rev:
CTAGTAGAATCACCACGACCTTCCGGGCCCGCACCAGCGCCGGCAGAGGTA
CATTTG

The following unphosphorylated oligonucleotides were annealed to form the 3′ pair:

C_for:
CTAGTCGTGGTGATTCTGCCGGCGCTGGTGCGGGCCCGGAAGGTACAAGCT
GTA

C_rev:
AGCTTACAGCTTGTACCTTCCGGGCCCGCACCAGCGCCGGCAGAATCACCA
CGA

pETA was double-digested with *Bam*HI and *Hin*dIII, and the ELP insert was double-digested with NheI and SpeI. Along with the two oligonucleotide pairs, these four components were ligated in a 1:6:6:6 molar ratio.

Genes in pETA plasmids were transformed into the *Escherichia coli* strain Tuner (DE3). Overnight cultures (5 mL) were used to inoculate expressions in Terrific Broth (1 L) under Kanamycin selection. Expression was induced with 0.5 mM IPTG at an OD_{600} = 0.9–1.1, and cells were harvested by centrifugation 6 h postinduction. Cell pellets were suspended in nondenaturing lysis buffer (MENT buffer: 10 mM Tris, 1 mM EDTA, 100 mM NaCl, pH = 7.5, 5 mM $MgCl_2$) at a concentration of approximately 30 g wet cell mass (WCM) per 100 mL buffer. Resuspensions were stored at −20 °C.

After thawing on ice, lysozyme (100 mg per 100 mL resuspension) was added, then after approximately 1 h the suspension was sonicated. Cell debris was removed by centrifugation, and DNase I and RNase A (2 mg each) were added to the clarified supernatant and incubated for 2–3 h at 37 °C. The turbid lysates were then centrifuged at 37 °C, and the pellets were redissolved in MENT buffer at 5 °C, typically overnight. The protein solutions were thermally cycled between 5 and 37 °C in MENT buffer for two additional cycles. The solutions were then dialyzed against ultrapure water and purified in a final step by passing over anion exchange resin in 6 M urea, 20 mM Tris, pH = 8.0, using HiTrap Q prepacked columns (GE Healthcare) by automated chromotography. Bound contaminants were discarded, and the target proteins were collected in the flow-through step, dialyzed against ultrapure water, and lyophilized.

Temperature–Concentration (*T*–*c*) State Diagram Construction

Hydrogel samples were prepared in ultrapure water. Turbidimetry was performed using a 662 nm 20 mW laser, on samples sealed in quartz with a 1 mm thick Teflon spacer and 2 mm bore. Samples were heated on a water-chilled brass stage at a heating rate of 1 °C/min. A TA Instruments Discovery Differential Scanning Calorimeter was used to perform DSC measurements. Samples were swollen in ultrapure water and loaded into hermetically sealed aluminum pans, and measurements were collected from 0–60 °C at a rate of 10 °C/min for two cycles followed by one cycle at 1 °C/min. The heat flow signal for the chain-extended ELP gels was insufficient to determine the onset of the transition at 1 °C/min, so T_t are reported from the second heating ramp at 10 °C/min. DSC measurements at 1 °C/min on unextended ELP gel samples resulted in transition temperatures (T_t) that deviated by less than 1 °C from the 10 °C/min ramp. Rheological T_t were determined as the point when $G' > G''$ at $\omega = 100$ rad/s.

Oscillatory Shear Rheology

Linear oscillatory shear rheology experiments were performed on an Anton-Paar MCR-702 rheometer operating in single-motor configuration in pseudostrain control (Direct Strain Oscillation) mode. Sample temperature was controlled using a Peltier heating element below

the lower geometry and a circulating air environmental enclosure to minimize thermal gradients across the sample. Measurements were performed with a 10 mm diameter, 2° cone-and-plate sample geometry, where the gap was zeroed at 37 °C and corrected for thermal expansion. Moduli were reported following a 30 min equilibration, at $\omega = 100$ rad/s and $\gamma_0 = 0.01$ unless otherwise noted.

Large amplitude oscillatory shear (LAOS) measurements were performed on the MCR-702 operating in dual-motor (TwinDrive) mode for true strain-control. Temperature was controlled using a circulating-air chamber. A 10 mm diameter, 2° cone-and-plate sample geometry with sandblasted surfaces was used. The gap was zeroed at 37 °C and corrected for thermal expansion. Samples were loaded at 0 °C and equilibrated for 20 min, then ramped up to 37 °C and equilibrated for 1 h prior to the start of the experiments. Strain sweeps were performed at $\omega = 1$ rad/s and cyclic sweeps were performed to increase maximum strain amplitudes with no waiting between cycles. The quality of the strain control was verified by evaluating the harmonic ratios of both the input strain and shear rate waveforms (Supporting Information). A cutoff of 1% in the fifth harmonic ratio (γ_5'/γ_1') was used to determine the range of valid strain amplitudes for LAOS analysis. Waveforms were analyzed with MITlaos v2.2 beta.[34,35]

Small Angle Scattering

Small angle X-ray scattering (SAXS) measurements were performed at the 12-ID-B beamline at the Advanced Photon Source at Argonne National Lab, with an X-ray wavelength of 13.998 Å and acquisition time of 0.02 s. 1D reductions were performed using beamline software and corrected for empty cell and solvent backgrounds. Samples were swollen in ultrapure water or 100 mM sodium phosphate, pH = 7.6. Measurements were performed on samples that had been equilibrated for at least 2 h on ice, then transferred to a prewarmed brass sample holder at 37 °C. Following the loading procedure, multiple measurements were taken at 10 min intervals, and no changes in nanostructure could be resolved. Fitting of the chain-extended scattering data was performed using software written in IGOR Pro made available by NIST.[36]

Tensile Testing

Samples were directly shaped into dogbones using a split Teflon mold 1 mm thick with a 3 mm gauge length machined with a water jet (Supporting Information). The split mold was coated in a thin layer of mineral oil, was held together with a rigid aluminum centering plate, and chilled on ice. Liquefied samples were loaded and then clamped between two Teflon sheets supported on brass plates. Samples were chilled on ice for at least 30 min, and then transferred to a forced air incubator at 37 °C and equilibrated for at least 8 h. Tensile measurements were performed at room temperature (22 ± 1 °C) on a Zwick Z2.5 linear mechanical tester with a 20 N load cell, at an engineering strain rate of 0.033 s^{-1}.

Erosion Tests

Samples were loaded into plastic molds with a laser-engraved cylindrical well 5 mm in diameter and 1 mm deep (Supporting Information). Hydrogels were prepared at 20 wt % in ultrapure water and completely dissolved on ice. Approximately 30 μL of gel was scooped

into a well, incubated on an aluminum plate held at 0 °C to liquefy, and then warmed to room temperature to solidify. Samples were transferred to scintillation vials, 10 mL of water prewarmed to 37 °C was added, and the vials were sealed with Parafilm to prevent evaporation. Vials were transferred to a 37 °C forced-air incubator for the duration of the experiment. Gel erosion was measured gravimetrically to the nearest 10 μg, with measurements performed in triplicate (i.e., dry off the mold, weigh, return to water, and then repeat twice more) for each sample replicate (N = 4) at each time point.

Release Tests

Hydrogels were prepared at 20 wt % in solutions of ultrapure water containing FITC-dextran particles (Sigma) at 1 mg/mL. Samples were loaded into plastic molds as described in the erosion experiment, and 4 mL of prewarmed water was added to each vial at the start of the experiment. Measurements of released dextran molecules were performed by extracting 100 μL at each time point, buffering the samples to 50 mM sodium phosphate, pH = 7.6, and measuring the fluorescence at excitation/emission wavelengths of 470/530 nm. Measurements were performed on three independent samples.

2D Cytocompatibility Testing with Human Mesenchymal Stem Cells (hMSCs)

Lyophilized ELP was hydrated at 20 wt % in sterile Dulbecco's Phosphate-Buffered Saline (PBS; Cat. No: 14190, Life Technologies) at 4 °C until the ELP solid was completely dissolved, fully hydrated, and transparent. Hydrated ELP samples in sterile Eppendorf tubes (VWR) were then transferred into an ice bath within a cell culture hood for seeding or encapsulation.

Untreated glass slides (48300-025, VWR) were cut into ~12.5 × 12.5 mm squares, and a 5 mm diameter circle was etched on the surface of the glass slide (depth ~100 μm) with a laser cutter (Universal Laser System, VLS2.30) to roughen the surface and improve hydrogel adhesion. The glass was washed with ethanol and exposed to cell culture UV for 20 min. Etched glass slides were placed on a metal substrate on the surface of the ice bath. Chilled 20 wt % ELP hydrogel was added to the center of the etched glass slide and flattened by adding the weight of another cut glass slide (~12.5 × 12.5 mm) on top of the ELP hydrogel. The system was allowed 1 min to flatten. The sample was then removed from the ice bath and warmed to room temperature, at which point the glass slides were pulled apart, leaving the ELP on the etched glass slide. The ELP-coated etched glass slide was then placed in a 12 well plate containing PBS with 1% penicillin/streptomycin (Life Technologies, Cat. No: 15140-122). All samples were incubated overnight (37 °C, 5% CO_2). PBS was removed and the samples were incubated for 30 min in the respective media prior to seeding hMSCs. hMSC cultures were trypsinized with 1% trypsin (0.5% EDTA, 10X, 15400-054, Life Technologies). Cell pellets were suspended in MSC media at a concentration of 1×10^6 cells/mL. 20 000 cells/well were added to 12 well plate wells containing either ELP-coated etched glass slides or similarly sized cut glass slides. Samples were incubated for 24 h with MSC media. After 1 day, the MSC media was replaced with either standard media (10% fetal bovine serum (FBS) (10437-028, Life Technologies) in DMEM media (Life Technologies)), 1% penicillin streptomycin (15140-122, Life Technologies) or

osteoinductive media (PT-3924 and PT-4120, Lonza). Additional details on reagents and cells are provided in the Supporting Information.

Bovine Chondrocyte Encapsulation

Twenty-eight weight percent ELP hydrogels were fully hydrated in sterile Eppendorf tubes (VWR) with sterile PBS at 4 °C. After hydration, the tube was transferred into an ice bath within a cell culture hood. Bovine chondrocytes were rapidly thawed from cryopreserved ampules (14 million cells/mL) in a 37 °C water bath. The cells were pipetted into 4 mL warm chondrocyte media [Hi-glucose DMEM (11965-092, Life Technologies), 1% sodium pyruvate (100 mM, 11360-070, Life Technologies), 1% nonessential amino acids (100X, 11140-050, Life Technologies), 1% HEPES buffer (1 M, pH 7.2, sterile filtered), 1% penicillin/streptomycin, with proline added at the time of seeding (400 μM in DMEM, Sigma-Aldrich), ascorbate (20 μg/mL in water, Sigma-Aldrich), and 10% FBS]. Twenty microliters of the cell suspension was used for cell counting by trypan blue staining. The cells were centrifuged (200 × *g*, 4 °C, 5 min) and suspended in chondrocyte media. The cell suspension was added to the ELP hydrogel at a concentration to yield a cell concentration of 1×10^7 chondrocytes/mL ELP hydrogel and an ELP solid concentration of 20 wt %. The chondrocyte ELP gel mixture was placed on a glass slide on a chilled metal substrate to liquefy and flatten. Another glass slide was placed on top of the ELP hydrogel with 150 um spacers (No. 1.5 coverslip, VWR) separating the glass slides to generate a uniform thickness hydrogel. After the hydrogel was flattened, the hydrogel was placed in the incubator for 5 min to solidify. It was then removed and cut into ~3 × 3 mm squares with a surgical blade and placed in 12-well plate wells containing chondrocyte media. Media was replaced after 24 h and then replaced every 3–4 days. Chondrocytes that were not mixed into the gels were seeded into 6 well plate wells at 100 000 cells/well and cultured overnight in chondrocyte media to characterize the cell population prior to encapsulation.

RESULTS AND DISCUSSION

Toughening of Gel-Forming ELPs by Oxidative Chain Extension

Gelation of the modified ELP sequence, denoted C-$([I^{0.6}V^{0.4}]PAVG)_{50}$-C, was found to proceed in a similar manner to the unmodified polypeptide: at sufficiently high concentrations, stiff gels were formed upon heating. Oxidation of the thiol moieties of the cysteine residues allows them to self-react to form disulfide linkages, and because only two cysteines are engineered into each protein (one near each terminus), these linkages allow for chain-extension of the ELP[27,32,33] (Figure 1a,b). While the gels without chain extension were brittle, the gels with chain extension were observed to be extensible and exhibit rapid recovery to their molded shapes. These improvements in gel toughness due to chain-extension are clear in tension, resulting in significant improvements in gel extensibility (Figure 1c). While gels made from $([I^{0.6}V^{0.4}]PAVG)_{50}$ are too brittle to be extended, C-$([I^{0.6}V^{0.4}]PAVG)_{50}$-C gels equilibrated at 37 °C for 8 h can be extended to engineering strains greater than 620% ± 140%. The Young's modulus estimated from the initial slope is 1.6 ± 0.4 MPa (Figure S1). The linear range extends to less than 20% engineering strain, which is followed by a necking regime, and finally strain-stiffening prior to failure.

These changes in mechanical properties are likely due to the presence of topological entanglements between polymers in the ELP-rich regions of the gel. Previously, increasing the molecular weight of polypeptides without chain-extension was observed to result in stiffer hydrogels,[15] suggesting that the increase in high molecular weight species in the oxidized C-($[I^{0.6}V^{0.4}]$PAVG)$_{50}$-C gels play a critical role in the mechanical performance of these arrested networks. Increasing toughness is also commonly observed in polymeric materials upon increasing molar mass above the entanglement molar mass. Protein gels (Figure 1c) show that high molar mass species are achieved in the oxidized ELPs, potentially yielding topological entanglements within the protein-rich regions and, consequently, the observed increases in gel toughness and extensibility.

To quantify the gelation conditions for both chain-extended and monomeric sequences, *T*-*c* state diagrams were constructed from a combination of DSC, turbidimetry, and rheological measurements. These diagrams reveal that the chain-extended ELP forms gels as low as 5 wt %, roughly similar to the unmodified sequences (Figure 2a,b). This gelation concentration, c_{min}, is half of that previously reported for a related but less hydrophobic sequence ($[I^{0.2}V^{0.8}]$PAVG)$_{50}$, where c_{min} was 15 wt %.[15] The shear moduli of these gels at $\omega = 100$ rad/s was found to range from 5 kPa at c_{min} to over 1 MPa at 30 wt %, with no substantial difference in the high frequency mechanics observed at high temperature due to chain-extension (Figure 2c). Solutions of ($[I^{0.6}V^{0.4}]$PAVG)$_{50}$ at 30 wt % transition from thin liquids to 7 MPa gels from 0 to 37 °C, while chain extension results in viscoelastic liquids (presumably due to chain entanglement at low temperature) that transition to 3 MPa gels over the temperature range.

Despite these similarities, the temperature- and frequency-dependence of the viscoelastic moduli suggest that network formation in chain-extended ELPs is modified as compared to the unextended sequences (Figure 3a,b). Solutions of C-($[I^{0.6}V^{0.4}]$PAVG)$_{50}$-C are more viscous than those of ($[I^{0.6}V^{0.4}]$-PAVG)$_{50}$ at low temperatures, exhibiting a crossover at high frequency (near $\omega = 100$ rad/s) for concentrations around 20 wt %. For ($[I^{0.6}V^{0.4}]$PAVG)$_{50}$ gels, a narrow stiffening transition is observed upon heating above the DSC-determined T_t, with a slower evolution of modulus nearer to 37 °C. Upon heating, C-($[I^{0.6}V^{0.4}]$PAVG)$_{50}$-C exhibits a significantly broader transition, characterized by a 5 °C difference between where G' becomes greater than G'' and where G'' begins to increase (Figure 3b). This broad, apparent two-step transition spanning nearly 10 °C is potentially related to the broad molecular weight distribution in the population of chain-extended species in C-($[I^{0.6}V^{0.4}]$-PAVG)$_{50}$-C gels, as ELPs are generally known to exhibit a molecular weight dependence of the apparent T_t. This result is consistent with the broader transition observed by DSC (Figure 3b insets). Frequency sweeps at 37 °C reveal the distribution of relaxation times in the chain-extended ELP gels is very similar to the unextended ELP gels (Figure 3c,d). This result is reasonable because the longest experimentally accessible relaxation time is governed by the kinetic arrest of the network, obscuring the effect of entanglements on the linear viscoelastic properties of the gels.

Effect of Chain-Extension on Gel Nanostructure

SAXS measurements reveal that arrested phase separation in gels prepared from chain-extended ELPs leads to a distinct nanostructure compared with gels formed from the unextended polypeptides alone. However, gelation of both polypeptides resulted in bicontinuous networks. Gels from concentrated solutions of $([I^{0.6}V^{0.4}]PAVG)_{50}$ at 37 °C exhibit scattering characteristic of a random two-phase system with sharp domain interfaces, evidenced by a broad peak at low wavevectors followed by power law decay with an exponent of −4 (Figure 4a).[15] The interdomain correlation length scale decreases with increasing gel concentration, as indicated by the peak shifting to higher wavevectors, without perturbing the Porod law scattering at high wavevectors. The qualitative picture is substantially different for gels from concentrated solutions of C-$([I^{0.6}V^{0.4}]$-$PAVG)_{50}$-C, which exhibit no peak over the observed *q*-range, no clear Porod regime, and exhibit a shoulder at high wavevectors (i.e., over the range 0.08 $Å^{-1} < q < 0.2$ $Å^{-1}$).

The concentration dependence of the scattered intensity distributions for the $([I^{0.6}V^{0.4}]PAVG)_{50}$ gels is consistent with a phase separation process that arrests when a critical local polypeptide concentration is reached (Figure 4b), as previously reported.[15] To estimate this concentration for dynamic arrest, the volume fraction of the dense polypeptide phase can be estimated from the invariant, *Q*, based on evidence of sharp domain interfaces in the Porod regime, according to

$$Q=(\rho_1-\rho_2)^2\phi_1(1-\phi_1) \quad (1)$$

where ρ_i is the X-ray scattering length density in phase *i*, and φ_1 is the volume fraction of the dense phase. Assuming that the ELP accumulates entirely in the dense phase, the scattering length density in each phase can be reasonably approximated by

$$\rho_1=\rho_{\mathrm{ELP}}\frac{\phi_{\mathrm{ELP,\ gel}}}{\phi_1}+\rho_{\mathrm{H2O}}\left(1-\frac{\phi_{\mathrm{ELP,\ gel}}}{\phi_1}\right) \quad (2)$$

$$\rho_2=\rho_{\mathrm{H2O}} \quad (3)$$

where $\varphi_{\mathrm{ELP,gel}}$ is the overall gel concentration and ρ_{H2O} and ρ_{ELP} are the X-ray scattering length densities of the pure components. This calculation reveals a nearly linear dependence of φ_1 on the overall mass fraction of the gel. The origin of this can be seen by calculating the concentration of polypeptide in the dense phase, $\varphi_{\mathrm{ELP},1} = \varphi_{\mathrm{ELP}}/\varphi_1$, which is nearly constant with an average value of 0.45. This result suggests that polypeptide densification during phase separation arrests when a critical concentration is reached. This concentration is likely related to protein sequence and thermal processing history, but that it remains constant is consistent with phase separation arresting due to slowing of chain reorganization, which is necessary for further coalescence of the nanoscale domains above a critical concentration.

For unextended ELP gels from $([I^{0.6}V^{0.4}]PAVG)_{50}$ at 37 °C, the data were fit to the clipped random wave (CRW) model,[37–40] which offers a simplified description of random inhomogeneous two-phase media. This model has been successfully applied to investigate the arrested phase separation of these ELPs,[15] in addition to bicontinuous microemulsions[41]

and phase separating polymer blends[42] (Figure 5a–c, Table 2). The CRW model is parametrized by three length scales that describe interdomain and intradomain correlations as well as interfacial curvature for random two-phase media with arbitrary composition. The power law slope, *n*, is fit directly to the experimental data, while the curvatures are computed from the parameters *a*, *b*, and *c* from the CRW model fits (Table S3). Prior to fitting, the absolute intensity distributions were corrected to account for thermal density fluctuations in random two-phase inhomogeneous systems, which manifest as a slight positive deviation in the background-corrected scattering curves above ca. $q \approx 0.3$ Å^{-1} (Figure 4a).[43] An empirical procedure for fitting an even power-law to the high *q* region according to the Vonk method accounts for this scattering well, leading to the expected pure monotonic decay in all scattered intensity distributions down to the level of experimental noise (Figure S2).[44] This scattering feature is not present in the scattered intensity for solutions at 5 °C, consistent with the origin of this positive deviation being in phase separated systems as opposed to polymer solutions.

Modeling of the scattering from $([I^{0.6}V^{0.4}]PAVG)_{50}$ gels indicates that their structure is consistent with bicontinuous, nanoscale networks with porosity that depends on gel concentration. Increasing overall gel concentration results in a more compact network, as indicated by a decrease in the interdomain correlation length (Figure 5c), consistent with the increased volume fraction of the polypeptide-rich phase from the Porod analysis. While the intradomain correlation length also decreases, the ratio $2\pi b/a$ is roughly constant, suggesting that the relative order quality of the domains does not change with concentration.[45] However, the interfacial curvature remains essentially constant with concentration and in all cases the Gaussian curvature, $\langle K \rangle$, is negative, consistent with a bicontinuous structure. The total interfacial area, related to S/V, is positively correlated with concentration across the studied range, indicating that high curvature is maintained even when arrest occurs at higher dense-phase volume fractions.

For the chain-extended gels, the CRW model fails to describe the scattered intensity distributions, but analysis of the general scattering features reveals evidence of fractal aggregation. Instead of a broad peak, the intermediate-*q* region ($q \sim 0.01$–0.04 Å^{-1}) in chain-extended gels appears to exhibit a decay characterized by an exponent between −2 and −3, which suggests scattering from a mass fractal. On the length scales suggested by this *q*-range, this type of behavior might be expected from the fractal aggregation of nanoscale building blocks, where the form factor of these building blocks is potentially evident at high *q*. The scattered intensity distributions for the chain-extended gels across all concentrations are nearly superimposable above $q > 0.02$ Å^{-1}, suggesting that the structure of these building blocks is very similar under the conditions investigated.

Given this combination of structural features, the scattered intensity distributions for C-$([I^{0.6}V^{0.4}]PAVG)_{50}$-C gels were fit to a fractal model with a form factor for nanoscale building blocks of polydisperse core-shell spheres.[36,46] This structure is envisioned as a dense core of ELP surrounded by a lower density layer. This model consists of parameters describing the volume fraction, φ, sphere core radius, R_{block}, sphere core polydispersity, σ_{block}, shell thickness, T_{shell}, fractal dimension, D_f, and network correlation length, ξ. This model was found to describe the scattering well across all concentrations (Figure 5d,e). The

model predictions support the observation that changing gel concentration does not strongly perturb the structure of the building blocks of the network and instead influences the effective density of these blocks as they form a percolating network. Crucially, the model predicts that the fractal dimension of the gel does not exhibit significant differences for the samples investigated, suggesting that the self-similar arrangement of building blocks is not significantly changed as a function of concentration.

This modeling provides an important description of the structure of these chain-extended gels and how it differs from the unextended sequences. Specifically, chain-extension changes both the form of the gel building blocks as well as their arrangement into a fractal percolating network, contrasting the two-phase network with sharp interfaces that forms from the assembly of the unextended sequences. Neither the form factor of the building blocks nor the fractal dimension of the aggregating network is perturbed significantly by the overall gel concentration (Figure 4). Instead, the average cluster size in the arrested state is larger at lower gel concentrations, indicative of a more porous gel (Figure 5f).

Diffusion of labeled biomolecules through the hydrogels supports the conclusion that they form bicontinuous networks with nanoscale pores. FITC-labeled Dextran molecules were encapsulated in both $([I^{0.6}V^{0.4}]PAVG)_{50}$ and C-$([I^{0.6}V^{0.4}]$-$PAVG)_{50}$-C gels and their release rates were measured fluorometrically (Figure 6). A clear size dependence of release was observed, with rapid and statistically similar release occurring for molar masses below 10 kDa within the first 20 h, and substantially slower release rates for larger Dextran. For both gels, these release rates suggest a broad distribution of pore sizes; however, in the case of the chain-extended ELP gels, there is a much greater size dependence in release rate, especially for Dextran greater than 10 kDa. In particular, 500 kDa Dextran exhibits negligible release over the course of the experiment, indicating that rearrangements of the physical network structure occur on extremely slow time scales consistent with rheological measurements. However, decreasing overall gel concentration to 7.5% improves the release rate of 500 kDa Dextran significantly due to increasing pore size, consistent with SAXS modeling of the chain-extended gels (Figure 5).

Nonlinear Mechanics and Recovery in Oscillatory Shear

C-$([I^{0.6}V^{0.4}]PAVG)_{50}$-C gels are compressible and extensible, exhibiting rapid recovery to their original shapes after moderate deformation, while $([I^{0.6}V^{0.4}]PAVG)_{50}$ gels are extremely brittle, as has been determined previously.[15] To characterize the effect of chain-extension on nonlinear mechanics, the gels were tested in large amplitude oscillatory shear (LAOS) rheology, which allows for interpretation of the viscous and elastic contributions during high strain perturbations. The behavior of the first harmonic of the stress response (G_1', G_1'', and σ_1; Figure 7a,b) reveals that the chain-extended ELP gels experience two nonlinear regimes. In the first regime, the gels appear to strain soften, but the stress amplitude continues to increase with increasing strain amplitude. In the second regime, the stress amplitude drops significantly with increasing strain amplitude, and the gels do not recover to their original performance unless liquefied by cooling to 0 °C and then reheated. Compared with the previous studies on the brittle unextended gels, the chain-extended gels are clearly tougher in shear.[15] In particular, the peak stress in the chain-extended gels occurs

at approximately $\gamma_0 = 3$ at either concentration, which is over an order of magnitude greater than what is observed for the unextended networks. This result is similar to the effect of increasing ELP molecular weight in unextended gels, where strain at peak stress is seen to increase from roughly $\gamma_0 = 0.1$ to 1 when the molecular weight is increased from 23 kDa to 53 kDa, at constant amino acid composition and gel concentration.[15]

While the gels fail irreversibly after strain amplitude sweeps to $\gamma_0 = 5.0$, cyclic strain amplitude sweeps indicate that the gels can recover following nonlinear oscillatory perturbations to intermediate strain amplitudes below $\gamma_{0,max} = 2.5$. Elastic Lissajous-Bowditch plots of the LAOS waveforms at increasing (+) and decreasing (−) strain amplitudes in a cyclic sweep reveal complex intracycle nonlinearities that are not captured by the behavior of the first harmonic alone. Thus, to understand in more detail the nonlinear response and recovery, the LAOS waveforms at various strain amplitudes were processed to extract the first order measures of elastic (G_M', G_L') and viscous nonlinearities (η_M' and η_L') for each individual oscillation cycle.[34,47] The ratios of these two parameters provide measures of the intracycle stiffening/softening $(S=[(G_L^{'} - G_M^{'})/G_L^{'}])$ and thickening/thinning $(T=(\eta_L^{'} - \eta_M^{'})/\eta_L^{'}))$. Furthermore, the proximity to perfectly plastic behavior can be assessed by computing the ratio of energy dissipated in a LAOS cycle compared to that of a perfectly plastic yield stress material over the same range cycle $\phi \equiv (\pi\gamma_0 G_1^{''}/4\sigma_{max})$.[48]

Examining the behavior of these parameters during a single sweep to failure reveals that chain-extension results in tough networks characterized by reduced dissipation at large strain amplitudes (Figure 8). In general, the behavior of *S* and *T* in both chain-extended gels (at 10 and 20 wt %) is similar to that of gels from unextended, high molecular weight ELPs.[15] The transition to the first nonlinear regime is characterized by substantial strain stiffening ($S > 0$) beyond $\gamma_{0,max} = 0.1$, and shear thinning ($T < 0$) is observed at large strain amplitudes for both gels. In addition, the chain-extended ELP gel exhibits a regime of slight shear thickening just at the transition point to the first nonlinear regime, although this is not observed at a concentration of 10 wt % (Figure 8b). However, at both concentrations, the chain-extended ELP gels exhibit relatively less dissipation than unextended ELPs when comparing the magnitude of φ. Furthermore, for the chain-extended ELP gels, φ actually decreases above $\gamma_0 = 0.5$, suggesting that the gels exhibit substantial elasticity well into the nonlinear regime.

Analysis of the strain amplitude dependence of the intracycle nonlinearities indicates that the chain-extended ELP gels recover well for perturbations less than $\gamma_{0,max} = 2.5$. While the first harmonic G' and G'' exhibit hysteresis between increasing and decreasing strain sweeps (Figure 7c,d), minimal hysteresis is observed in *S* and *T* (Figure 8). While the hysteresis loop in φ is non-negligible, the increasing strain sweeps are essentially superimposable, indicating that the gel recovers after the oscillatory perturbations decrease to within the linear regime. This behavior is in contrast to the behavior of unextended, high molecular weight ELP gels,[15] which have shortened linear viscoelastic ranges after oscillatory shear above $\gamma_{0,max} = 0.1$, indicating the accumulation of irreversible damage to the network. While in tension the chain-extended gels plastically deform and cannot return to their original macroscopic dimensions, large amplitude oscillatory shear rheology indicates that

chain-extension leads to improved recovery of the gel network after nonlinear shear deformation as well as minimal hysteresis during cycling in shear.

Biomaterial Performance in Vitro

In vitro assessment of these arrested physical networks reveals their long-term persistence in solution at 37 °C (Figure 9), an important property for in vivo applications where early degradation of physical gels by erosion poses an important limitation. Gel erosion was evaluated in water for gels prepared at 20 wt %, and $([I^{0.6}V^{0.4}]PAVG)_{50}$ gels exhibited no measurable mass loss over the time periods investigated, appearing to slightly swell over the course of 1 week. While the chain-extended gels lost approximately 20% of their mass prior to the first measurement (at 6 h), the gels were stable for longer time periods (Figure 9). This rapid initial mass loss is likely due to the gel shrinking (deswelling) rather than erosion, given the long-term stability of the stiff gel after extended equilibration in excess water at 37 °C.

The high modulus, improved toughness, and easy preparation of the chain extended gels makes them attractive as responsively tough matrices for tissue regeneration, particularly in load-bearing tissues such as cartilage or bone. In addition to the benefits of implanting void-filling gels that can rapidly convert into stiff ($G' \sim 1$ MPa) and robust materials, matrix elasticity has been shown to control the phenotype of MSCs, with stiff substrates supporting osteogenic differentiation.[49] To investigate the cytocompatibility of the biofunctionalized, chain-extended gels and determine their potential to be used in the engineering of stiff tissues, 20 wt % gels of C-$([I^{0.6}V^{0.4}]PAVG)_{50}$-C were initially explored as substrates for 2D seeding of hMSCs. These sequences contained two cell-adhesive RGDS peptides genetically fused near the N- and C-termini of the ELP, one on each side. As the moduli of these networks are greater than 1 MPa, experiments were performed in media without osteogenic molecules to assess the ability of the substrates to support osteogenesis. The gels were prepared in water, washed in PBS, and soaked in media prior to seeding. They exhibited no significant decay throughout the experimentation, consistent with erosion measurements performed in pure water. Seeded cells demonstrated good attachment, remaining viable out to 21 days postseeding (Figure 10a,b). Osteogenesis was inferred by examining the alkaline phosphatase activity of the gels at day 21 compared with cells seeded on the tissue culture plate in media without osteogenic molecules and osteoinductive media (Figure 10b; Figure S7). Alkaline phosphatase is a secreted enzyme whose activity is associated with bone formation and typically suggestive of osteogenesis.[50,51] While alkaline phosphatase activity was less than that observed for hMSCs seeded on glass slides in osteoinductive media by day 21 (Figure S7), the cells expressed greater alkaline phosphatase activity distributed throughout the gel compared with the control, consistent with weak osteogenesis. Image quantification indicates approximately a 2-fold increase in activity over the control, not as potent as the 9-fold increase in activity observed under osteoinductive conditions. Immunohistochemical staining for osteocalcin and osteopontin expression, noncollagenous proteins (NCPs) found in the extracellular matrix (ECM) of bone,[50,51] supports this conclusion (Figure 10c). Similar to alkaline phosphatase expression, hMSCs seeded on top of the gels exhibit greater production of these markers of osteogenesis compared in the absence of the gel, although not as strong as in osteoinductive media. Image quantification

indicates a 2-fold increase in osteopontin expression and a 30-fold increase in osteocalcin expression over the control in the gel, compared with a 20-fold and 6-fold increase in osteopontin and osteocalcin expression under osteoinductive conditions. Distinct expression profiles during osteogenic differentiation and bone mineralization serve to explain the higher expression of osteocalcin in cells undergoing differentiation[52] on the gels. Cells under stronger osteoinductive stimulation and potentially undergoing active mineralization show increased alkaline phosphatase[53] and osteopontin[54] activity.

Because of the ability to rapidly transition from a viscoelastic liquid to an extremely stiff gel with a mild shift in temperature, primary cell isolates of bovine chondrocytes can also easily be mixed into these gels. To achieve a final concentration of 20 wt %, the gels were prepared at 28 wt % in PBS to minimize potential osmotic shock when the suspended chondrocytes were mixed with the viscoelastic fluid. Cells and the ELP were then mixed to a final ELP concentration of 20 wt % and a cell density of 1×10^7 chondrocytes/mL. The gels were prepared with a thickness of 0.4 mm, and seeded chondrocytes were viable (86% viability) and retained their rounded morphology throughout 28 days of incubation[55] (Figure 10d, Figure S8).

CONCLUSIONS

High-performance biomaterials that are responsive, robust, and easy to formulate are critical to address challenges in tissue engineering and regenerative medicine. Through this work, an arrested phase separation mechanism for forming extremely stiff physical networks from ELP solutions is shown to be amenable to telechelic modifications of the polypeptide, including oxidatively-coupling cysteine residues for gel toughening and cell-adhesive RGDS peptides for bioactivity. Chain-extended ELP gels were significantly tougher in shear and extension than the brittle unextended ELP gels. Furthermore, chain-extension modifies the arrested phase separation process, resulting in fractal networks of nanoscale aggregates that are bicontinuous with a broad pore size distribution. These gels exhibited excellent erosion resistance, and the networks were cytocompatible with hMSCs in 2D as well as chondrocytes mixed into the gels. The ability to formulate an easily manipulated liquid solution that can immediately solidify upon heating to an extremely stiff, erosion-resistant gel with a protein sequence similar to natural extracellular matrix components has important implications in the design of new substrates for the regeneration and engineering of stiff tissues in vivo. Thus, the ability to form thermoreversible biomaterials compatible with processing techniques needed for cellular encapsulation in complex implant architectures offers many new opportunities to prepare high-performance matrices for engineering and regenerating load-bearing tissues.

Supplementary Material

Refer to Web version on PubMed Central for supplementary material.

Acknowledgments

This research was supported by the U.S. Army Research Office under contract W911NF-07-D-0004. The authors would like to acknowledge Dr. Xiaobing Zuo for his assistance at the 12-ID-B beamline at the Advanced Photon

Source at Argonne National Lab, Dr. Boualem Hammouda from the Center for Neutron Research at NIST for helpful discussions, and Christopher Lam for machine shop assistance. We would also like to acknowledge Dr. Simona Socrate for the use of her tensile tester, as well as Prof. Randy Ewoldt and Prof. Gareth McKinley for access to the MITlaos software.

References

1. Place ES, Evans ND, Stevens MM. Nat Mater. 2009; 8(6):457–470. [PubMed: 19458646]
2. Peppas NA, Hilt JZ, Khademhosseini A, Langer R. Adv Mater. 2006; 18(11):1345–1360.
3. Macaya D, Spector M. Biomed Mater. 2012; 7(1):012001. [PubMed: 22241481]
4. Kretlow JD, Klouda L, Mikos AG. Adv Drug Delivery Rev. 2007; 59(4):263–273.
5. Van Tomme SR, Storm G, Hennink WE. Int J Pharm. 2008; 355(1):1–18. [PubMed: 18343058]
6. Drury JL, Mooney DJ. Biomaterials. 2003; 24(24):4337–4351. [PubMed: 12922147]
7. Wong Po Foo CTS, Lee JS, Mulyasasmita W, Parisi-Amon A, Heilshorn SC. Proc Natl Acad Sci U S A. 2009; 106(52):22067–22072. [PubMed: 20007785]
8. Olsen BD, Kornfield JA, Tirrell DA. Macromolecules. 2010; 43(21):9094–9099. [PubMed: 21221427]
9. Fisher JP, Jo S, Mikos AG, Reddi AH. J Biomed Mater Res. 2004; 71A(2):268–274.
10. Macaya DJ, Hayakawa K, Arai K, Spector M. Biomaterials. 2013; 34(14):3591–3602. [PubMed: 23414684]
11. Kretlow JD, Young S, Klouda L, Wong M, Mikos AG. Adv Mater. 2009; 21(32–33):3368–3393. [PubMed: 19750143]
12. Burdick JA, Anseth KS. Biomaterials. 2002; 23(22):4315–4323. [PubMed: 12219821]
13. Thornton AJ, Alsberg E, Hill EE, Mooney DJ. J Urol. 2004; 172(2):763–768. [PubMed: 15247778]
14. Tsitsilianis C. Soft Matter. 2010; 6(11):2372–2388.
15. Glassman MJ, Olsen BD. Biomacromolecules. 2015; 16:3762. [PubMed: 26545151]
16. Urry, D.; Luan, CH.; Harris, CM.; Parker, TM. Protein-Based Materials. Springer; New York: 1997. p. 133-177.
17. MacEwan SR, Chilkoti A. Biopolymers. 2010; 94(1):60–77. [PubMed: 20091871]
18. Kim W, Chaikof EL. Adv Drug Delivery Rev. 2010; 62(15):1468–1478.
19. Wright ER, Conticello VP. Adv Drug Delivery Rev. 2002; 54(8):1057–1073.
20. Urry DW. J Phys Chem B. 1997; 101(51):11007–11028.
21. McDaniel JR, Radford DC, Chilkoti A. Biomacromolecules. 2013; 14(8):2866–2872. [PubMed: 23808597]
22. Gong JP, Katsuyama Y, Kurokawa T, Osada Y. Adv Mater. 2003; 15(14):1155–1158.
23. Myung D, Waters D, Wiseman M, Duhamel PE, Noolandi J, Ta CN, Frank CW. Polym Adv Technol. 2008; 19(6):647–657. [PubMed: 19763189]
24. Gudeman LF, Peppas NA. J Appl Polym Sci. 1995; 55(6):919–928.
25. Gaharwar AK, Dammu SA, Canter JM, Wu C-J, Schmidt G. Biomacromolecules. 2011; 12(5): 1641–1650. [PubMed: 21413708]
26. Gaharwar AK, Peppas NA, Khademhosseini A. Biotechnol Bioeng. 2014; 111(3):441–453. [PubMed: 24264728]
27. Tang S, Glassman MJ, Li S, Socrate S, Olsen BD. Macromolecules. 2014; 47(2):791–799. [PubMed: 24910474]
28. Gong JP. Soft Matter. 2010; 6(12):2583–2590.
29. Haque MA, Kurokawa T, Kamita G, Gong JP. Macromolecules. 2011; 44(22):8916–8924.
30. Sun TL, Kurokawa T, Kuroda S, Ihsan AB, Akasaki T, Sato K, Haque MA, Nakajima T, Gong JP. Nat Mater. 2013; 12(10):932–937. [PubMed: 23892784]
31. Waters DJ, Engberg K, Parke-Houben R, Ta CN, Jackson AJ, Toney MF, Frank CW. Macromolecules. 2011; 44(14):5776–5787.

32. Yuan S, Hollinger M, Lachowicz-Scroggins ME, Kerr SC, Dunican EM, Daniel BM, Ghosh S, Erzurum SC, Willard B, Hazen SL, et al. Sci Transl Med. 2015; 7(276):276ra27–276ra27.
33. Gerrard JA. Trends Food Sci Technol. 2002; 13(12):391–399.
34. Ewoldt RH, Hosoi A, McKinley GH. J Rheol. 2008; 52(6):1427–1458.
35. Cho KS, Hyun K, Ahn KH, Lee SJ. J Rheol. 2005; 49(3):747–758.
36. Kline SR. J Appl Crystallogr. 2006; 39(6):895–900.
37. Chen S-H, Chang S-L, Strey R. J Appl Crystallogr. 1991; 24(5):721–731.
38. Chen S-H, Choi S. Supramol Sci. 1998; 5(3):197–206.
39. Choi, SM.; Chen, SH. Formation and Dynamics of Self-Organized Structures in Surfactants and Polymer Solutions. Springer; New York: 1997. p. 14-23.
40. Choi, SM.; LoNostro, P.; Chen, SH. Trends in Colloid and Interface Science XIII. Springer; New York: 1999. p. 98-104.
41. Chen S, Chang S, Strey R, Samseth J, Mortensen K. J Phys Chem. 1991; 95(19):7427–7432.
42. Jinnai H, Hashimoto T, Lee D, Chen S-H. Macromolecules. 1997; 30(1):130–136.
43. Perrin P, Prud'Homme RE. Macromolecules. 1994; 27(7):1852–1860.
44. Vonk C. J Appl Crystallogr. 1973; 6(2):81–86.
45. Chen SH, Lee DD, Kimishima K, Jinnai H, Hashimoto T. Phys Rev E: Stat Phys, Plasmas, Fluids, Relat Interdiscip Top. 1996; 54(6):6526–6531.
46. Teixeira J. J Appl Crystallogr. 1988; 21(6):781–785.
47. Hyun K, Wilhelm M, Klein CO, Cho KS, Nam JG, Ahn KH, Lee SJ, Ewoldt RH, McKinley GH. Prog Polym Sci. 2011; 36(12):1697–1753.
48. Ewoldt R, Winter P, Maxey J, McKinley G. Rheol Acta. 2010; 49(2):191–212.
49. Engler AJ, Sen S, Sweeney HL, Discher DE. Cell. 2006; 126(4):677–689. [PubMed: 16923388]
50. Anselme K. Biomaterials. 2000; 21(7):667–681. [PubMed: 10711964]
51. Sikavitsas VI, Temenoff JS, Mikos AG. Biomaterials. 2001; 22(19):2581–2593. [PubMed: 11519777]
52. Nakamura A, Dohi Y, Akahane M, Ohgushi H, Nakajima H, Funaoka H, Takakura Y. Tissue Eng Part C. 2009; 15(2):169–80.
53. Golub EE, Boesze-Battaglia K. Cur Op Orthop. 2007; 18(5):444–448.
54. Sodek J, Ganss B, McKee MD. Crit Rev Oral Biol Med. 2000; 11(3):279–303. [PubMed: 11021631]
55. Takahashi T, Ogasawara T, Asawa Y, Mori Y, Uchinuma E, Takato T, Hoshi K. Tissue Eng. 2007; 13(7):1583–92. [PubMed: 17630901]

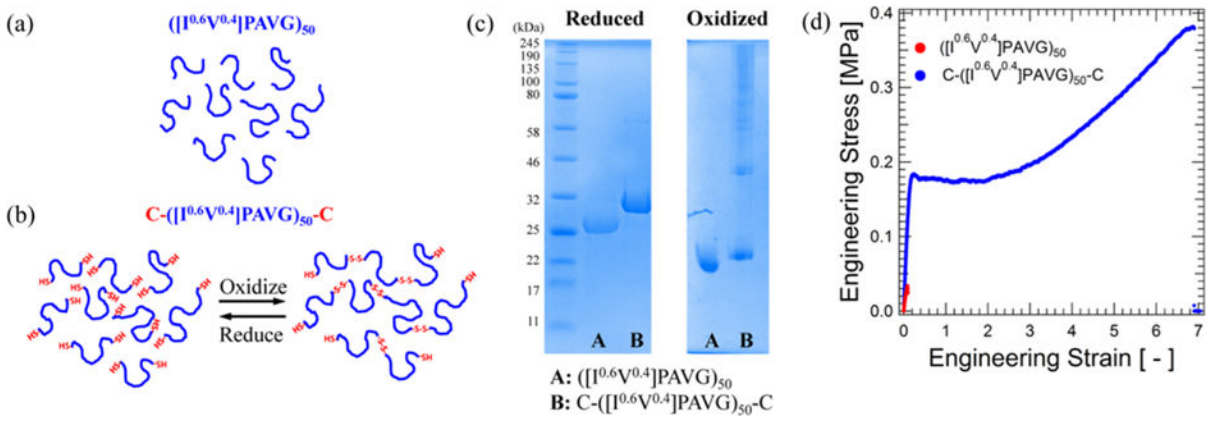

Figure 1.

Schematic of solutions of the (a) unextended ELP and (b) oxidatively chain-extended ELP. (c) Reducing and nonreducing SDS-PAGE demonstrating the broad molecular weight distribution of the oxidized cysteine-functionalized ELP. (d) Uniaxial tension on gels prepared at 20 wt % in water. Samples were equilibrated at 37 °C prior to experimentation at room temperature at 0.1 mm/s (engineering strain rate of 0.033 s^{-1}).

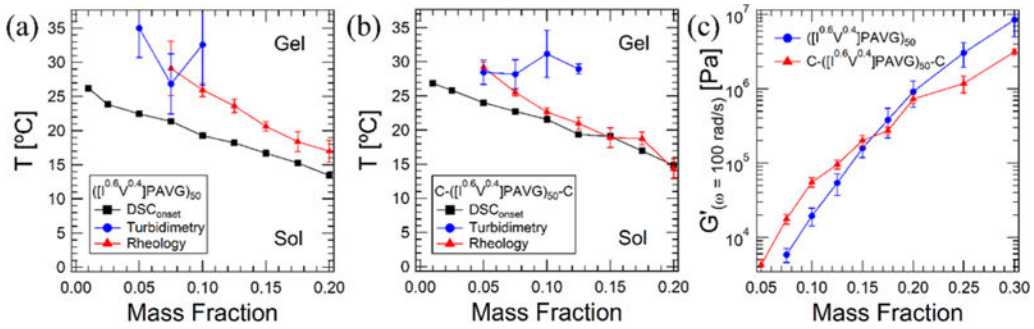

Figure 2.

T-c state diagrams for (a) $([I^{0.6}V^{0.4}]PAVG)_{50}$ and (b) chain-extended C-$([I^{0.6}V^{0.4}]PAVG)_{50}$-C. (c) Comparison of the high frequency elastic modulus ($G'[\omega =$ 100(rad/s)]) for gels under various conditions to examine the effect of telechelic modifications on the linear viscoelastic properties. Measurements were taken at T = 37 °C after 30 min equilibration following a 1 °C/min heating ramp, at γ_0 = 0.01.

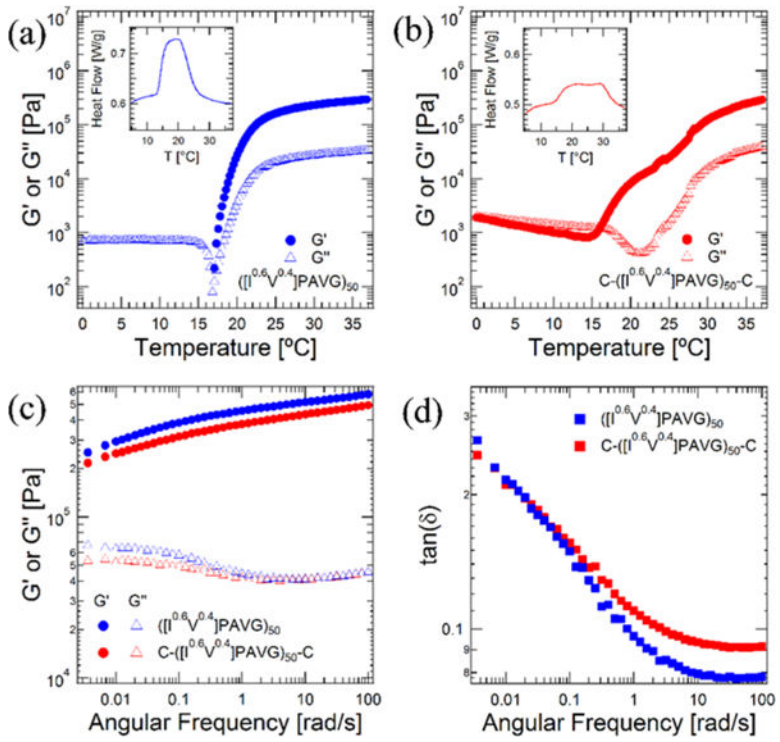

Figure 3.

Effect of chain extension on the linear viscoelasticity of 20 wt % gels. Temperature ramp experiment (ω = 100 rad/s, γ_o = 0.01, dT/dt =1 °C/min) on (a) ([$I^{0.6}V^{0.4}$]PAVG)$_{50}$ and (b) C-([$I^{0.6}V^{0.4}$]PAVG)$_{50}$-C gels. Insets show DSC heating ramps at 10 °C/min. Comparison of the frequency dependence of (c) the viscoelastic moduli and (d) tan(δ) at 37 °C.

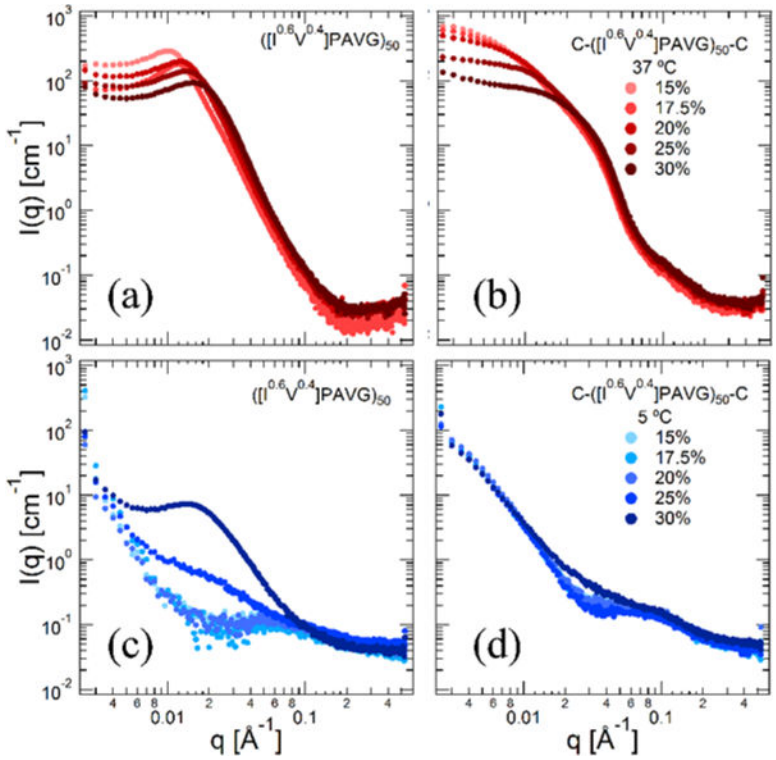

Figure 4.

SAXS intensity distributions for (a,c) $([I^{0.6}V^{0.4}]PAVG)_{50}$ and (b,d) C-$([I^{0.6}V^{0.4}]PAVG)_{50}$-C at 37 and 5 °C, respectively.

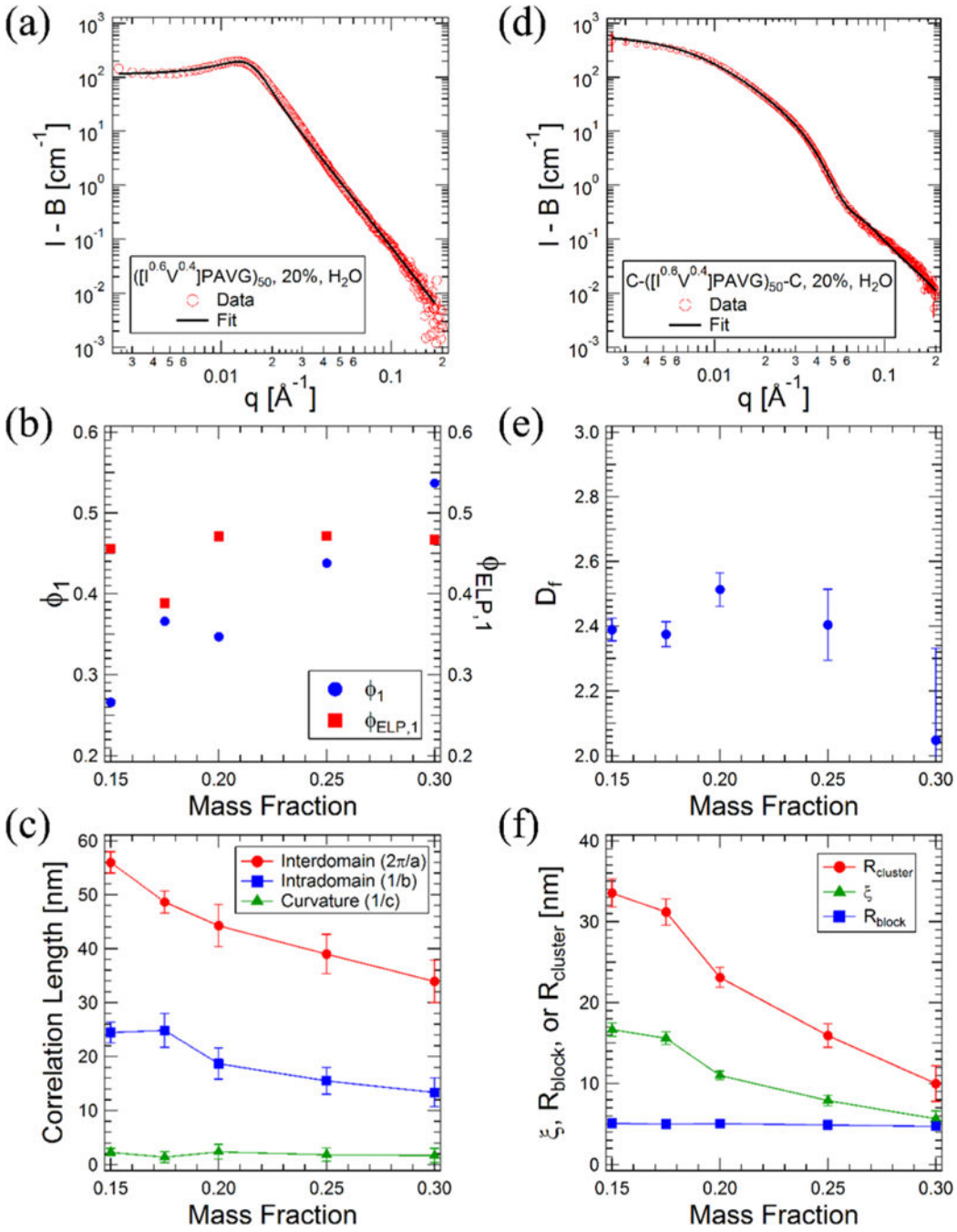

Figure 5.

Modeling of the SAXS intensity distributions for (a–c) ([I$^{0.6}$V$^{0.4}$]PAVG)$_{50}$ and (d–f) C-([I$^{0.6}$V$^{0.4}$]PAVG)$_{50}$-C. (a) Example of Vonk-corrected data for 20 wt % ([I$^{0.6}$V$^{0.4}$]PAVG)$_{50}$ gels fit to the clipped random wave model. (b) Porod analysis of the ELP concentration in the dense phase. (c) Correlation length scales fit to the CRW model. (d) Example of Vonk-corrected data for 20 wt % C-([I$^{0.6}$V$^{0.4}$]PAVG)$_{50}$-C gels fit to the model for fractal aggregation of polydisperse core-shell spheres. (e) Fractal dimension of chain-extended gels from the model fits. (f) Gel correlation length scales from the model fits.

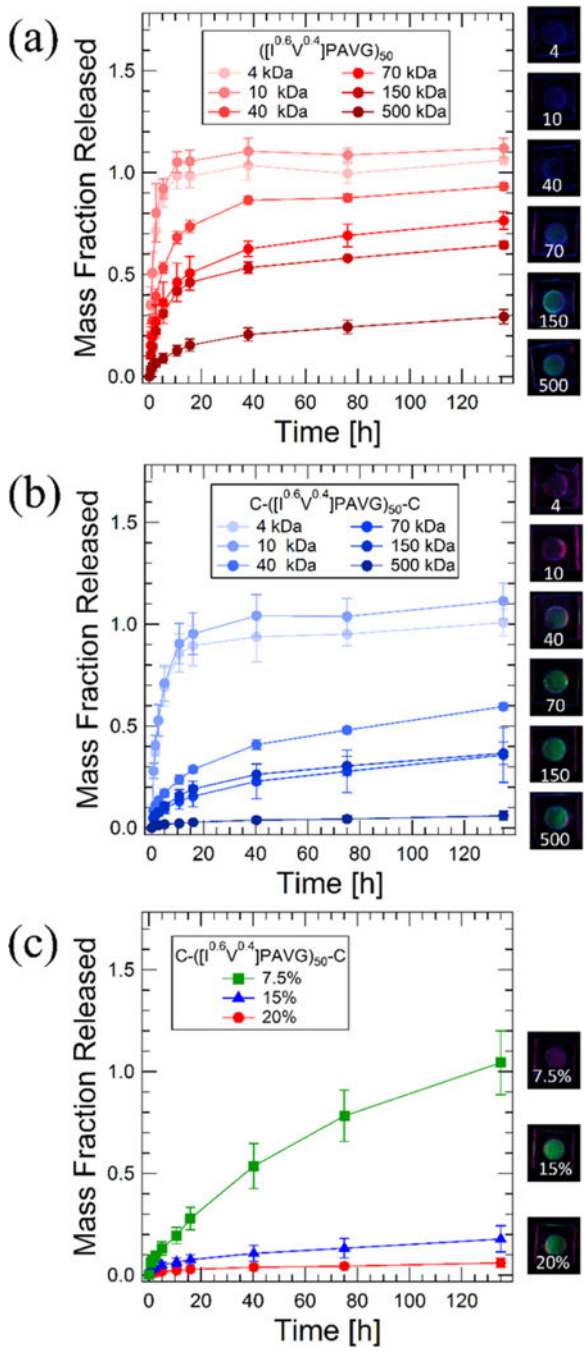

Figure 6.

Release studied from gels at 20 wt % with 0.1% Dextran from 4 kDa to 500 kDa in (a) $([I^{0.6}V^{0.4}]PAVG)_{50}$ and (b) C-$([I^{0.6}V^{0.4}]$-$PAVG)_{50}$-C gels. (c) Release of 500 kDa Dextran from C-$([I^{0.6}V^{0.4}]$-$PAVG)_{50}$-C as a function of concentration from 7.5 to 20 wt %. Images show residual Dextran in the gels at the final time point.

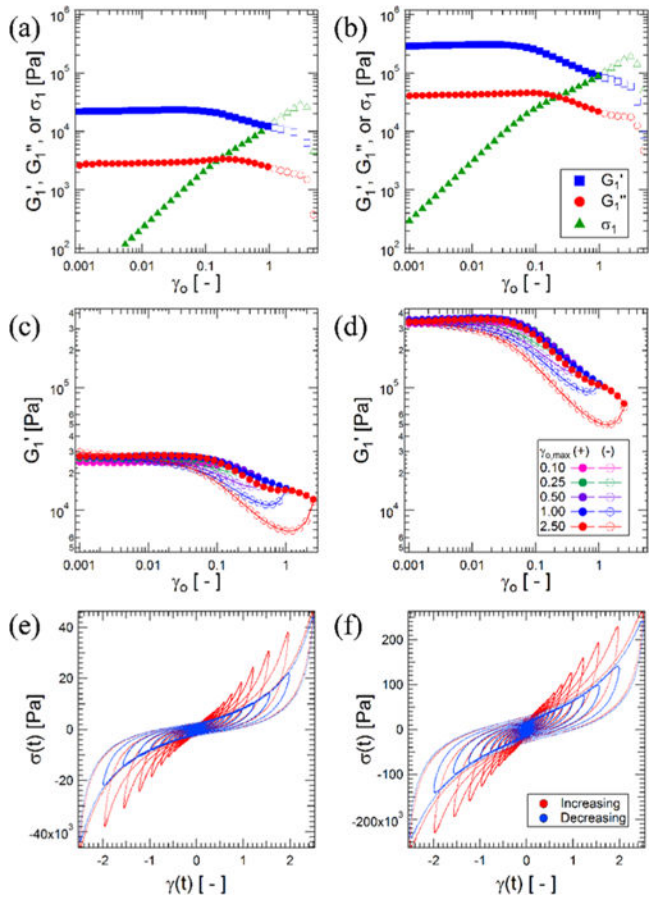

Figure 7.

Behavior of the first harmonic of the stress response as a function of increasing maximum strain amplitude into the nonlinear regime for C-([$I^{0.6}V^{0.4}$]PAVG)$_{50}$-C at (a) 10 wt % and (b) 20 wt % in H_2O at 37 °C. Data where the spectral purity of the shear rate waveform is between 0.01 and 0.03 are plotted as open symbols. Cyclic strain sweeps to increasing maximum strain amplitudes for C-([$I^{0.6}V^{0.4}$]-PAVG)$_{50}$-C at (c) 10 wt % and (d) 20 wt %. Elastic Lissajous-Bowditch plots for (e) 10 wt % and (f) 20 wt % gels during cyclic strain sweeps to a maximum strain amplitude, $\gamma_{o,max}$ = 2.5.

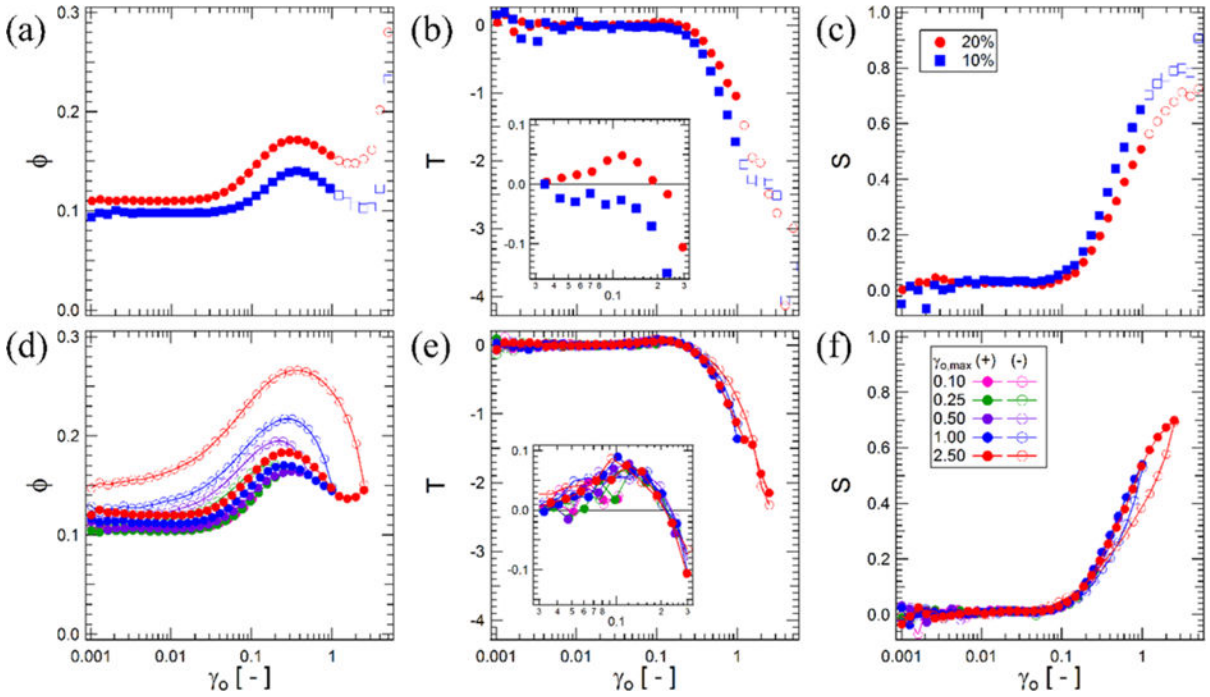

Figure 8.

Intracycle nonlinearities during a single strain sweep out to the maximum strain amplitude comparing the effect of gel concentration for C-([$I^{0.6}V^{0.4}$]PAVG)$_{50}$-C at 10 and 20 wt %: (a) perfect plastic dissipation ratio, (b) thickening ratio, and (c) stiffening ratio. Data where the spectral purity of the shear rate waveform is between 0.01 and 0.03 are plotted in open symbols. Intracycle nonlinearities during cyclic strain sweeps for 20 wt % C-([$I^{0.6}V^{0.4}$]PAVG)$_{50}$-C: (d) perfect plastic dissipation ratio, (e) thickening ratio, and (f) stiffening ratio.

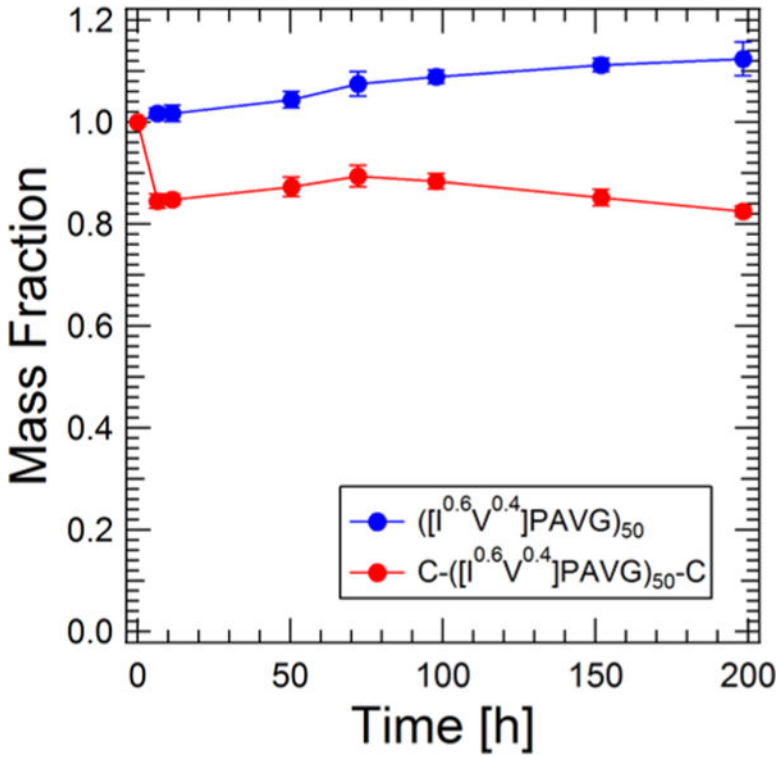

Figure 9.

Mass fraction remaining as a function of time measured gravimetrically from cylindrical wells (5 mm diameter, 1 mm deep, $N = 4$) in water at 37 °C.

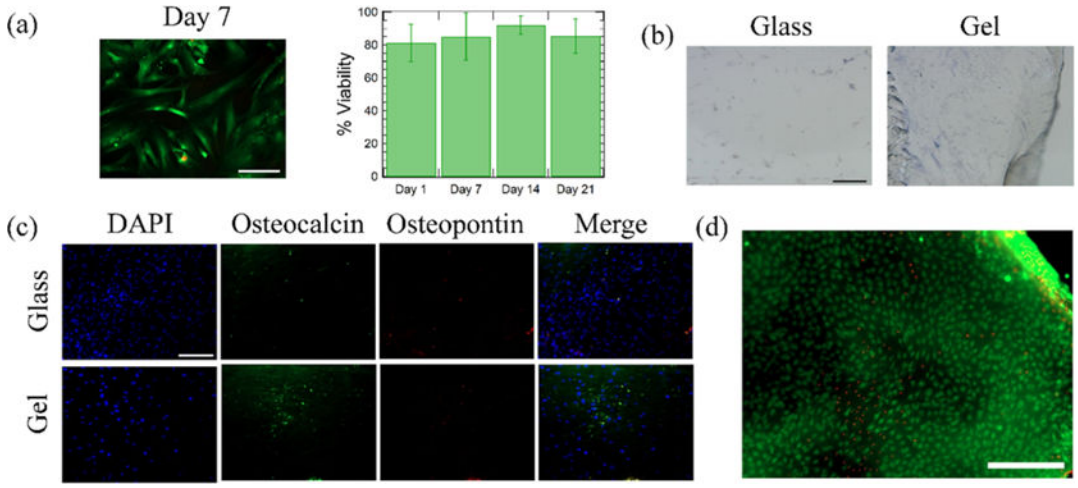

Figure 10.

hMSC viability and osteogenesis on C-([$I^{0.6}V^{0.4}$]PAVG)$_{50}$-C gels. (a) Cell viability: image of LIVE/DEAD staining on day 7 and quantified by cell counting in ImageJ. (b) Staining for alkaline phosphatase activity on day 21 for cells seeded directly on glass slides and onto the surface of the gel in standard cell media. (c) Immunohistochemical staining for osteocalcin and osteopontin expression. (d) Viability of bovine chondrocytes mixed with C-([$I^{0.6}V^{0.4}$]PAVG)$_{50}$-C gels after 28 days of incubation.

Table 1

ELP Sequences

notation	amino acid sequence	MW (
$([I^{0.6}V^{0.4}]PAVG)_{50}$ (single ELP chain)	MGWGSASGLVG $[(IPAVGVPAVG)_2(IPAVG)]_{10}$ ETTS	23
C-$([I^{0.6}V^{0.4}]PAVG)_{50}$-C (oxidatively coupled)	MGWGSKCTSAGAGAGPEGRGDSTSGLVG $[(IPAVGVPAVG)_2(IPAVG)]_{10}$ ETTSRGDSAGAGAGPEGTSCKL	26

Table 2

Curvature, Interface, and Order Quality Parameters for $([I^{0.6}V^{0.4}]PAVG)_{50}$ Gels

mass fraction	n	$\langle H \rangle$ [× 10^{-2} nm^{-1}]	$\langle K \rangle$ [× 10^{-3} nm^{-2}]	$\langle H^2 \rangle$ [× 10^{-2} nm^{-2}]	S/V [× 10^{-2} nm^{-1}]	$(2\pi b/a)$
0.15	−3.81 ± 0.08	3.80	−3.05	3.36	5.22	0.437
0.175	−3.85 ± 0.08	2.53	−6.59	7.95	7.33	0.511
0.20	−3.91 ± 0.05	2.78	−5.66	3.10	6.81	0.423
0.25	−3.89 ± 0.05	1.31	−9.41	5.19	8.73	0.397
0.30	−3.93 ± 0.04	−0.987	−12.2	6.16	9.93	0.394